Integration of Plasmonic Antenna on Quantum Cascade Laser Facets for Chip-scale Molecular Sensing

Dibyendu Dey, John Kohoutek, Ryan M. Gelfand, Alireza Bonakdar and Hooman Mohseni*
Bio-inspired sensors and optoelectronics laboratory
Department of Electrical engineering and Computer science
Northwestern University, Evanston, Illinois, USA 60208
*hmohseni@ece.northwestern.edu

***Abstract*— Many important bio-molecules, such as proteins and pharmaceuticals, have their natural resonances in the mid-infrared (2 - 30μm) region of the optical spectrum. The primary challenge of sensing these molecules is to increase the interaction between them and light with such long wavelengths. This can be overcome by exploiting optical nano-antennas which can squeeze the optical mode into a volume much smaller than the operating wavelength. We present a novel antenna design based on hybrid materials composed of a coupled Au-SiO_2-Au nanorod integrated on the facet of a quantum cascade laser (QCL) operating in the mid-infrared region of the optical spectrum. FDTD simulations showed that for sandwiched dielectric thicknesses within the range of 20 to 30 nm, peak optical intensity at the top of the antenna ends is 4000 times greater than the incident field intensity. The device was fabricated using focused ion beam milling. Apertureless mid-infrared near field optical microscopy (NSOM) showed that the device can generate a spatially confined spot within a nanometric size about 12 times smaller than the operating wavelength. Such high intensity, hot spot locations can be exploited to enhance the photon interaction for bio-molecules for sensing applications.**

I. Introduction

Since its first demonstration [1] in 1994, Quantum cascade laser (QCL) has shown path breaking performance in term of wall-plug efficiency [2, 3] and is currently considered as one of the most efficient sources in the mid-infrared (IR) region of optical spectrum. In its region of operation, several bio and chemical molecules has significant absorption and thus building bio sensors based on QCL is highly desired. But unfortunately due to several orders of magnitude dimensional difference between the lasing wavelength and the size of probed molecules, the light-particle interaction potential comes out to be very weak and it has remained the primary challenge in building a sensitive mid-IR bio-sensors. The problem can be overcome by using optical nano antennas [4,5], which are capable of focusing radiant infrared light down to nanometer lengths scale and strongly enhance the near field intensity. Previously demonstrated nano antennas integrated with QCL has shown strong near field enhancement but they were based on metal design [6, 7]. Here, we demonstrate a metal-dielectric-metal based coupled nanorod antenna integrated on the facet of a quantum cascade laser, which confines the optical mode within a nanometric spot size ~ 500nm. There is almost ~4 times intensity enhancement for MDM antenna design as opposed to the metal design. Multiple coupling mechanisms lead to this increased enhancement. MDM antenna also generates multiple hot spots due to geometrical singularities – a feature extremely useful for bio-sensing applications. After optimizing the design, we fabricated and measured the device using a custom designed near field microscope. We have used hybridization theory to explain measured field intensity of the antenna. Such integrated antenna can be used for bio-sensing applications [8]. Finally, we have also outlined the roadmap to build an efficient chip-scale molecular sensor based on the device.

II. Simulations

In order to accomplish the effective device design, we simulated the effect of each components of the integrated antenna using commercially available 3d FDTD software, Lumerical.

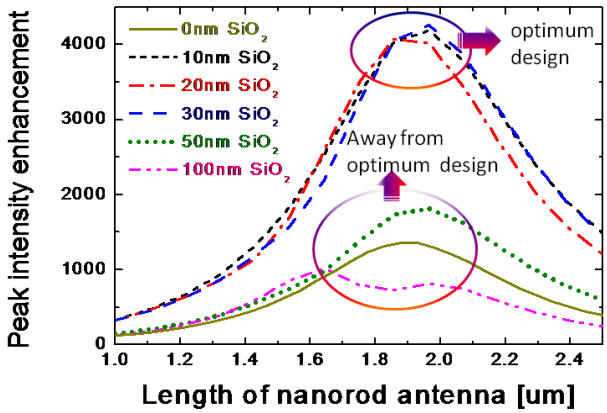

Figure 1 - FDTD simulation shows the peak intensity enhancement vs antenna length. The silicon dioxide thickness for MDM structure has been varied from 0, 5, 10, 20, 30 to 50 nm, while keeping the total thickness of the structure to be constant at 170nm.

All material data used in the simulation, other than the laser region, is from ref [9]. The refractive index of the laser material is chosen to be 3.2, which is the weighted average of the refractive index of the active region,$In_{0.44}Al_{0.56}As/In_{0.6}Ga_{0.4}As$. An optical TM polarized plane wave (natural resonance for QCL due to selection rule) with lasing wavelength at 5.97µm (found from the emission spectrum of the device) is used as the source for all performed FDTD simulations. At resonance, the surface charge is accumulated at the end of each nanorod and it is maximized at the gap between two closely placed nanorods due to capacitive coupling [10]. The accumulated charge leads to large electric field intensity enhancement at the vicinity of the gap [11].

In order to understand the effect of dielectric thickness on intensity enhancement, the SiO_2 thickness of the MDM antenna design has been varied from 0, 10, 20, 30, 50 and 100nm, while keeping the total thickness of composite MDM layer constant at 170nm. The simulated peak intensity enhancement at the antenna gap on the same level as the top surface is plotted against varying length of the antenna in Fig. 1. As the SiO_2 thickness is changed from 10 to 30 nm, there is a ~ 4-fold increase in peak optical intensity.

The physics of MDM antenna is substantially different compared to a single metal design. The near field intensity enhancement for MDM antenna involves multiple coupling processes. To further clarify, we have shown the simulated the electric field distribution for the MDM antenna in xz plane at y=0.

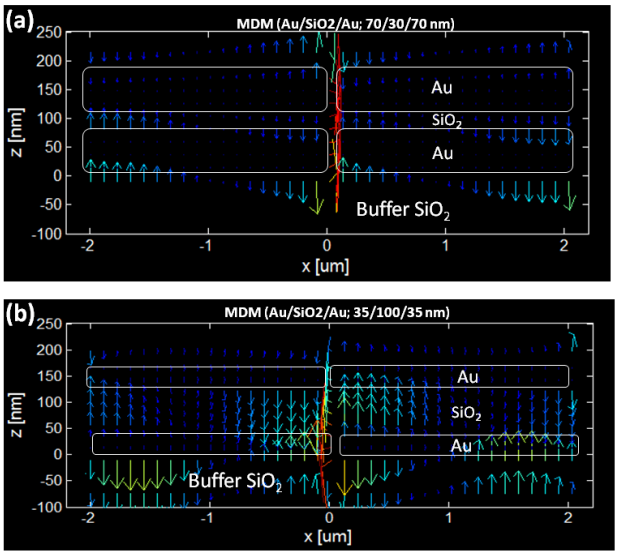

Figure 2 –E-field for MDM (70/30/70 nm) antenna at a resonance length L=2.0um for each nanorod. The sandwiched dielectric thickness is (a) 20nm and (b) 100nm whereas the total thickness of the structure is kept to be constant at 170nm.

At the beginning, the incident laser light generates surface plasmons on the bottom Au/buffer SiO_2 interface. Due to vertical plasmon coupling, surface charges are induced on the top Au and simultaneously a strong electric field is generated inside the sandwiched dielectric. From Figure 2(a)-(b), it can also be found that most of the electromagnetic field resides inside the sandwiched dielectric and thus there is little absorption loss due to the metal. Finally, the induced dipole moments at each vertically coupled Au antenna couple radiatively to generate strong near field enhancement. This could also be viewed in frequency domain (steady state) using coupled mode theory, which has been covered extensively in the literature [12].

Increasing the sandwiched dielectric thickness beyond optimum thickness leads to decoupling of top and bottom antenna. This can be well-understood comparing the E-field distribution of Fig-2 (a) and (b). At a sandwiched dielectric thickness of 100nm, most of the electric field is confined close to the bottom antenna. Thus in this case, the near field intensity drops near the top metal of the antenna.

III. FABRICATION

We fabricated a quantum cascade laser with nano-patterned antenna on the facet. Our QCL is based on $In_{0.44}Al_{0.56}As/In_{0.6}Ga_{0.4}As$ with a core design as outlined in a previous letter [13]. After cleaving, the lasers were mounted on a c-mount and tested for current-voltage performance at room temperature. After initial characterization, one facet of the device was coated with $SiO_2/Au/SiO_2/Au$ (100/70nm/30nm/70nm) by E-beam evaporation.

The nanorod antenna was then fabricated on the coated facet of the laser using a Focused Ion beam (Hellios FEI). Using the gallium ion beam at high voltage (30keV) and low current (48pA), a high precision of milling was achieved. The fabricated antenna on the facet of QCL is shown in Fig 3.

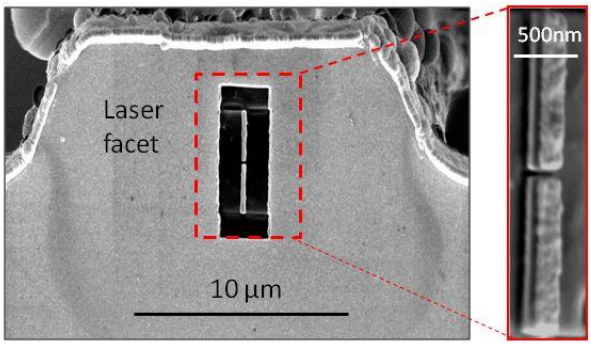

Figure 3- Scanning optical microscope (SEM) image of the Au-SiO_2-Au (75/30/75nm) coupled nanorod antenna integrated on the facet of quantum cascade laser. (Right side) Magnified SEM image showing the metal-dielectric-metal layers of the coupled antenna.

IV. MEASUREMENT

The laser was operated in pulsed mode with 1% duty cycle (100ns, 100 KHz). The threshold current was found to be 2.28A and 1.68A respectively with and without fabricated antenna. The reduction in threshold current is due to increasing reflectivity from the facet by the metal coating.

After fabricating the antenna integrated quantum cascade laser, we used an apertureless near field scanning optical microscope (NSOM) to probe it. In this technique, the near-field images and topography of the patterned QCL were

simultaneously measured. Commercially available NSOMs generally use a spatially confined optical spot at the end of a hollow metallic scanning tip to selectively illuminate the probed surface to produce an image beyond the diffraction limit. However, this set-up involves complicated intermediate optics and an external light source. In contrast, we have set up a mid-infrared NSOM (Fig. 4) based on a commercially available atomic force microscope (AFM) (Agilent 5400). The apex of the sharp platinum coated AFM tip scans the surface of the sample and scatters the local electromagnetic field coming from the antenna structure. The AFM cantilever was driven at its resonance oscillation frequency of 70 KHz. The scattered signal travels back through the laser cavity and after collimation through objective a lens, gets collected by a mercury-cadmium telluride (MCT) detector. This scattered signal possesses local field information. However, there is also scattering from the cantilever which produces a huge background noise. As the signal has a definite frequency band defined by the tapping mode frequency of the AFM, noise and signal can be separated using Lock-in technique with a matching reference frequency. The resulting signal gives an image of the near field intensity pattern of the fabricated antenna.

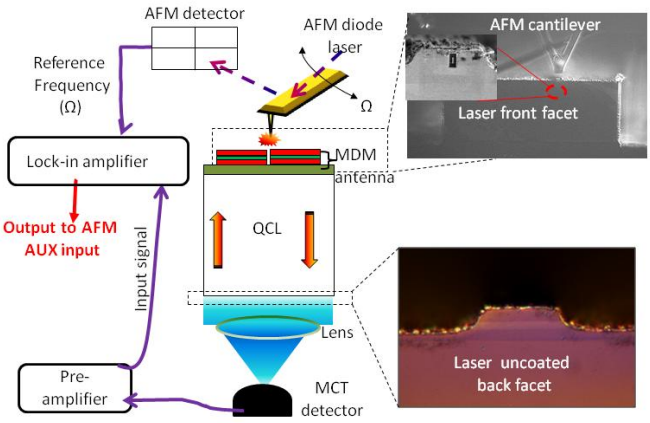

Figure 4 – Schematic diagram showing the near-field optical microscope (NSOM) set-up for simultaneously measurement of the topography and near-field intensity of MDM antenna integrated with QCL.

The antenna near fields excites SPs to the AFM tip, which in turn radiates a signal detected by infrared detector to generate NSOM image. In Fig. 5 (a) and (b), the topography and near field image of Au-SiO_2- Au (75/30/75nm) coupled nanorod antenna is shown. The full-width at half maximum (FWHM) of the center spot has been found to be ~ 450nm. In ref 14, a quasi-electrostatic theory has been used to calculate the radiated dipole field by the AFM tip and is found to be stronger for electric field perpendicular to the sample surface (E_z). Thus, there may be two other existing components of scattered electric field, E_x and E_y (in-plane), interact with the AFM tip, the E_z component of the near field is expected to be recorded predominantly. In Figure 4 (c), we have shown simulated E_z field intensity. Although the simulation showed maximum field intensity at both ends of the coupled antenna, experimentally measured NSOM data repeatedly showed two bright spots [15]. It is important to mention here that unlike a single metal design, the plasmon resonance in a complex structure like MDM coupled antenna is not straightforward. It requires a detailed hybridization theory to understand the plasmon resonance in a MDM coupled antenna and we have discussed it in a nutshell in the next section.

The near-field images of the antenna were recorded with high pixel resolution and with a reduced scan speed of 0.1 lines/s. The image distortions, as seen in Fig 5 (a)-(b), are due to small drifts in sample position occurring over the long acquisition time for NSOM measurement.

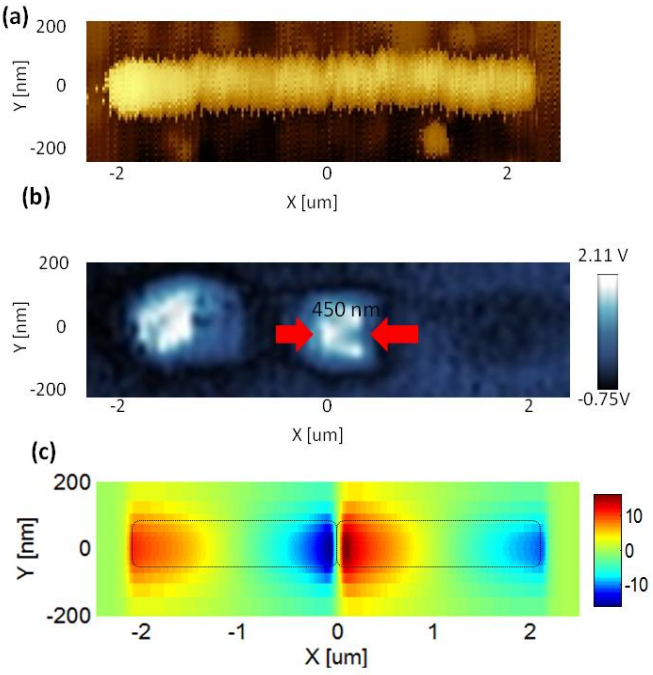

Figure 5 – (a)-(b) Topography and NSOM image of the coupled MDM nanorod antenna. The resonant length of each nanorod is ~2μm and the sandwiched dielectric is kept to be optimum ~ 30nm. (c) Top view of simulated E_z field along the antenna axis, 50nm above the top metal surface. The length and thickness parameters are same as above.

V. Discussion

Plasmon interaction and hybridization has been used to describe plasmon resonance in many complex structures, for example metallic nanoshell [16], stacked cut-wires [17] and sandwiched optical antenna [18]. In the following, we first apply the plasmon hybridization theory on a single MDM nanorod and subsequently use these analytic results to understand the more complicated design like coupled MDM nanorod.

Due to the presence of sandwiched dielectric, MDM single nanorod antenna can be considered as two vertically coupled metal antennas stacked together. The surface plasmon waves at the top and bottom antenna interact and split the resonance frequency (for single metal antenna). The generated surface plasmon modes are (a) Symmetric plasmon mode (ω^+) and (b) Antisymmetric plasmon mode (ω^-). The two modes correspond to the charge oscillation of the top and

bottom antenna in (symmetric) or out of phase (antisymmetric).

The two resonances can be found from the frequency spectrum of the single MDM antenna as shown in Fig 6(a). The different charge configuration for symmetric and antisymetric states have been shown in Fig 6(b). For symmetric mode, the charges at the end of the rod repels and leads to increased restoring force of charge oscillation compared to antisymmetric mode. Thus plasmon resonance energy of symmetric mode is higher. Further, for symmetric mode there is an effective dipole at both the ends of the nanorod, whereas it is zero for the antisymmetric mode.

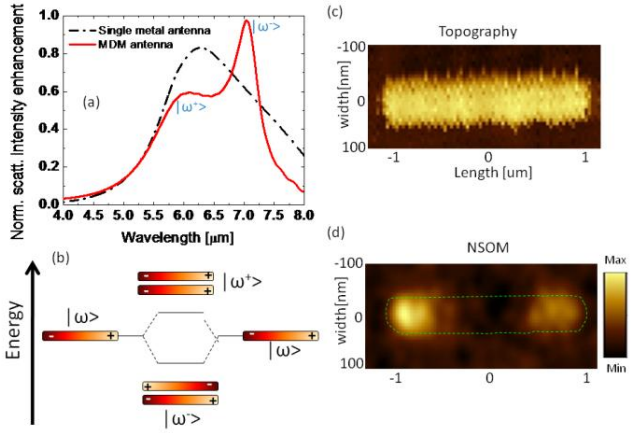

Figure 6 – (a) Spectrum of the MDM and single metal antenna showing the symmetric and antisymetirc Plasmon modes. (b) Schematic diagram of the charge configuration for the vertically coupled MDM single nanorod in different modes of resonance. (c) – (d) Topography and NSOM of the MDM single nanorod antenna at a resonance length of 2.05um

The symmetric resonance corresponds to the lasing wavelength ~ 6μm. The topography and NSOM measurement for MDM single nanorod are shown in Fig 6(c)-(d [19]. There are two bright hot spots have been observed as expected for a symmetric plasmon mode. The non-identical behavior of the two spots is due to non-uniformity on the top metal surface caused by FIB.

The analytical results of the single nanorod can now be applied to interpret plasmon responses for a more complex design such as coupled MDM nanorod. The hybridization of symmetric modes lead to two plasmon modes ω_s^+ and ω_s^- and similarly interaction of antisymmetric modes leads to another two plasmon modes ω_a^+ and ω_a^-. In principle there can also be coupling between symmetric and antisymmetric modes as been stated in ref [16]. The coupling leads to the charge configuration as shown in Fig. 7. In quasistatic limit, ω_{as} mode would have two bright regions since the net dipole moment is non-zero at only two regions. Thus anti-symmetric mode hybridization between the symmetric and anti-symmetric modes eventually leads to the two bright spots found in the NSOM measurement of MDM coupled nanorod.

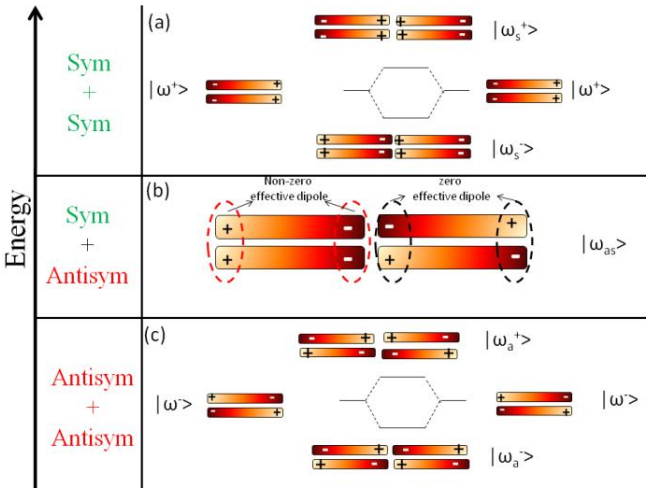

Figure 7 – Schematic illustration of the plasmon hybridization of two coupled MDM antenna.(a) Symmetric types plasmon modes.(b) Plasmon modes corresponding to interaction between symmetric and antisymmetric modes. (c) Antisymmetric type plasmon modes.

VI. Antenna Based Sensor

To be able to investigate bio-molecules, which have vibration frequency in the mid-infrared region of optical spectrum, the detection volume must be reduced by an order of magnitude. The QCL integrated optical antenna has shown squeezing of optical spot within a small volume (radius ~ 12 times smaller than the operating wavelength). Thus any bio or chemical molecule, which has vibration resonance matching the lasing frequency, can have a strong absorption while inside the confined spot size. Now the challenge comes to develop a process to load such molecules at specific location of the antenna where the near field enhancement takes place. Further, the loading process needs precise control so that it doesn't affect reflectivity of laser front facet (directly related with lasing performance).

We propose dip-pen nanolithography (DPN) [20, 21] process to load the antenna hot spot with bio/chemical molecules. In this technique, an atomic force microscope (AFM) tip is used to transfer molecule to the surface via a solvent meniscus. This technique allows direct deposition of nanoscale materials onto an antenna in a flexible manner. There are four steps involved in the sensing process as described in Fig.8. First the solution is prepared with the bio/chemical molecule at near saturation in a solvent with a low vapor pressure like acetonitrile or ethanol. Second, a clean AFM tip is dipped in the solution for 30s and then dried with compressed air. This process is repeated several times. After drying, the AFM tip is used in non-contact mode to find the nanoantenna and the exact location we want to deposit the molecules. The AFM is then switched into contact mode to deposit molecules in the region of the optical antenna where the hot spot is generated. Finally, the near field intensity of the antenna integrated QCL with the molecules is again measured in non-contact mode. This process can be repeated

as there is no deposition of material during the non-contact mode scans. So in this way we can load the cavity, measure the optical response and continue to load and measure the cavity to monitor how the amount of material affects the optical properties of this device. Here we only show our preliminary results of molecular deposition using dip-pen nanolithography (Fig.9). The deposition of molecules on the antenna and the corresponding NSOM measurement will be reported in future.

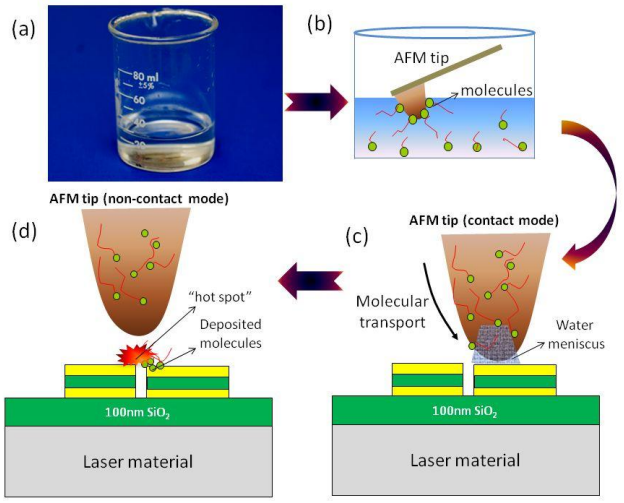

Figure 8 – 4 steps process of depositing and sensing bio-molecules using an optical antenna integrated QCL. (a) Preparation of bio/chemical molecular solution (b) Dipping the AFM tip and form a monolayer of molecules attached to it (c) loading the molecule at specific location of the antenna in contact mode of AFM (d) NSOM measurement of the molecule loaded QCL integrated antenna.

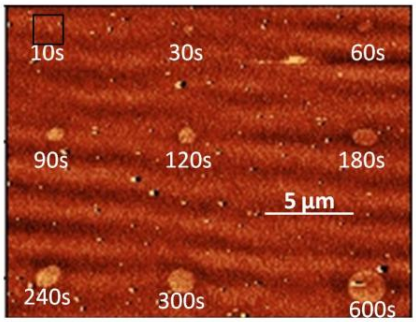

Figure 9 – Deposition of mercapto-hexadecanoic acid (MHA) on the surface of a gold-coated silicon wafer using dip pen nanolithography (DPN). The volume of deposited molecule is directly proportional to the deposition time. The image on the top left has minimum deposition time of 10s and bottom right has maximum deposition time of 600s. The scan sizes were 25µmx25µm, and the scan speed was 1Hz.

ACKNOWLEDGMENT

This project has been partially funded by NSF grant # CBET-0932611. The Focused Ion beam milling and SEM studies were performed in the (EPIC) (NIFTI) (Keck-II) facility of NUANCE Center at Northwestern University. NUANCE Center is supported by NSF-NSEC, NSF-MRSEC, Keck Foundation, the State of Illinois, and Northwestern University.

REFERENCES

[1] J. Faist, F. Capasso , D. L. Sivco , C. Sirtori , A. L. Hutchinson , and A.Y. Cho, "Quantum cascade laser," Science, vol. 264, pp. 553- 56, April 1994.

[2] Y.Bai, S. Slivken, S. Kuboya, S. R. Darvish and M. Razeghi, "Quantum cascade laser that emits more light than heat," Nat. Photonics, vol. 4, pp. 99-102, January 2010

[3] P. Q. Liu, A. J. Hoffman, M. D. Escarra, K. J. Franz, J. B. Khurgin, Y. Dikmelik, X. Wang, J.-Y. Fan and C. F. Gmachl, "High power efficient quantum cascade," Nat. Photonics, vol. 4, No. 98, January 2010.

[4] J. Alda, J. M. Rico-Garcia, J. M. Lopez and G. Boreman,"Optical antennas for nano-photonic applications," Nanotechnology, vol. 16, pp. S230-S234, March 2005.

[5] X. Xu, E. X. Jin, L. Wang and S. Uppuluri,"Design, fabrication and characterization of nanometer-scale ridged aperture optical antenna," Proc. SPIE., vol. 6106, pp.61061J-1-61061J-12, March 2006.

[6] N. Yu, E. Cubukcu, L. Diehl, M.A. belkin, K. B. Crozier and F. Capasso,"Plasmonic quantum cascade laser antenna," Appl. Phys. Lett., vol. 91, pp.173113-1-173113-3, October 2007.

[7] E. Cubukcu, N. Yu, E. J. Smythe, L. Diehl, K. B. Crozier and F. Capasso,"Plasmonic laser antenna and related devices," IEEE Journal of Selected Topics in Quantum Electronics, vol. 14, pp.1448 – 1461, December 2008.

[8] M. F. Garcia-Parajo,"Optical antenna focusing in on biology," Nature Photonics, vol. 2, pp. 201 – 203, April 2008.

[9] D. Palik, Handbook of Optical constants of solids,Academic Press, New York, 1985.

[10] E. Cubukcu, E. A. Kort, K. B. Crozier and F. Capasso, "Plasmonic laser antenna," Appl. Phys. Lett.,vol. 89, pp.093120-1-093120-3, August 2006.

[11] J. Aizpura, G. W. Bryant, L. J. Ritcher, F. J. G. De Abajo, B. K. Kelley, and T. Mallouk,"Optical properties of coupled metallic nanorods for field-enhanced spectroscopy,"Phys.Rev.B,vol.71,pp.235420-1-235420-13, Junuary 2005.

[12] L. Zhou, C. -P. Huang, S. Wu, X. -G. Yin, Y. -M. wang, Q.-J.Wang, and Y.-Y. Zhu,"Enhanced optical transmission through metal-dielectric-metal multilayers grating,"Appl.Phys.Lett.,vol.97,pp. 011905-1-011905-3, July 2010.

[13] L. Diehl, D. Bour, S. Corzine, J. Zhu, G. Hofler, M. Loncar, M. Troccoli and F. Capasso,"High-temperature continous wave operation of strain-balanced quantum cascade lasers grown by metal organic vapor-phase epitaxy," Appl. Phys. Lett., vol. 83, pp. 3245-47, October 2003.

[14] M. Knoll and F. Keilmann. "Enhanced dielectric contrast in scattering-type scanning near-field optical microscopy,". *Optics Communication* vol. 182, pp.321-328, Aug. 2000

[15] D.Dey, J. Kohoutek, R. M. Gelfand, A. Bonakdar and H. Mohseni,"Quantum cascade laser integrated with metal-dielectric-metal based plasmonic antenna," Opt. Lett., in press.

[16] E. Prodan, C. Radloff, N. J. Halas and P. Nordlander,"A hybridization model for the plasmon response of complex nanostructures,". Science, vol. 302, pp. 419-422, October 2003.

[17] N. Lie, H. Guo, L. Fu, S. Kaiser, H. Schweizer, and H. Giessen,"Plasmon hybridization in stacked cut-wires metamaterials," Adv. Mater., vol. 19, pp. 3628-3632, October 2007.

[18] L. Wang, J. Zhang, X. Wu, J. Yang and Q. Gong,"Resonances of sandwiched optical antenna," Opt. Comm.,vol. 281, pp.5444-5447, August 2008.

[19] D.Dey, J. Kohoutek, R. M. Gelfand, A. Bonakdar and H. Mohseni." Quantum cascade laser integrated with metal-dielectric-metal plasmonic antenna," SPIE.Proceeding, in press

[20] R. D. Piner, J. Zhu, F. Xu, S. Hong and C. A. Mirkin. "Dip-pen nanolithography," Science, vol. 283, pp. 661-663, January 1999.

[21] K.–B. Lee, S. –J. Park, C. A. Mirkin, J. C. Smith and M. Mrksich, "Protein nanoarrays generated by dip-pen nanolithography," Science vol. 295, pp. 1702-1705, February 2002.